MULTI-PARAMETER ROVER WHEEL AND GROUSER OPTIMIZATION FOR DEPLOYMENT IN PHOBOS' MILLI-G ENVIRONMENT

Virtual Conference 19–23 October 2020

Felix Buchele[1,2], Roy Lichtenheldt[2]

[1]Department of Mechanical Engineering, University of Applied Sciences Kempten,
Bahnhofstr. 61, 87435 Kempten, Germany, E-mail: buchelefelix@gmail.com
[2]Institute for System Dynamics and Control, German Aerospace Center (DLR),
Münchener Straße 20, 82234 Weßling, Germany, E-mail: roy.lichtenheldt@dlr.de

ABSTRACT

This paper investigates wheeled locomotion in milli-g environments and specifically the wheeled locomotion of a small rover which is supposed to be deployed on Phobos as part of the Martian Moons eXploration mission. Several wheel geometry parameters and driving scenarios are considered and are simulated using a Discrete Element Method tool. As a result, design guidelines for wheeled locomotion in milli-g environments are developed and the differences between locomotion in low gravity and high gravity environments are highlighted. Furthermore, an optimized wheel geometry for use on Phobos is presented.

1 INTRODUCTION

The Japanese Aerospace eXploration Agency (JAXA) is planning to explore the Martian moons Phobos and Deimos with a mission scheduled for launch in 2024. The Martian Moons eXploration Mission (MMX) aims to unveil the origin of the Martian moons, which is still a matter of controversy. There are two main theories on the origin of the two moons. The most significant theory assumes, that the moons are captured outer-belt asteroids. This theory is supported by remote-sensing data which suggests similarities between the moon's regolith and C- or D-type carbonaceous asteroids [1,2].

The second theory assumes the in-situ formation of the moons. They could have formed either along with the formation of Mars itself [3] or due to an impact event, that blasted debris into Mars' orbit, allowing in-situ formation. This theory is supported by the near-circular orbits of both moons, which are hard to explain assuming the moons were captured asteroids [1].

To determine the actual origin of Phobos and Deimos, the MMX probe is supposed to take samples of the Phobos regolith back to Earth for ex-situ examination. Additionally, the mission features a lightweight, wheeled rover for in-situ examination of Phobos and its surface. The rover furthermore serves a second purpose. Since the rover will land on Phobos before the probe does, it also secures and scouts the probe's landing site, reducing the hazards of its landing [4].

In order to achieve its goals, the rover has to be well prepared for the hazardous conditions of space in general and the challenging environment of Phobos in particular. Since Phobos is an airless celestial body, its surface is expected to be covered by a thick layer of loose regolith with a low density [5] and otherwise vastly unknown soil properties [6]. Furthermore, the surface gravity of Phobos is extremely low. The MMX rover will be in fact the first wheeled rover to operate under comparably low gravity.

1.1 Simulation Framework

Since the environmental conditions on Phobos are a completely new challenge for wheeled rover locomotion, it is necessary to examine, improve and adapt the rover's locomotion system. One of the major threats a planetary environment can pose to any wheel-driven rover is lack of traction. Especially on loose, sandy planetary soils, rover wheels might get stuck, rendering the rover immobile. NASA's Mars Exploration Rover (MER) missions show impressively that this is true. Both rovers struggled while traversing loose soils. While Opportunity managed to free itself from a sand trap [7], getting stuck in loose soil lead to the end of Spirit's mission [8].

To save the MMX rover from this fate, the rover's wheel geometry has to be adapted to the environment of Phobos. Wheel geometry examination and optimization for rover missions are often carried out by experiments (e.g. [9–11]). In this case, due to the huge differences in gravitational acceleration between Phobos and Earth, experimental evaluation is not suitable [12]. Therefore, a numerical Discrete Element Method (DEM) based approach is chosen for the optimization.

The software chosen to simulate the rover wheel and soil contact is partsival, a high-fidelity DEM simulation framework, developed by the German Aerospace Center (DLR). partsival is a well-tested tool and

suitable for various tool-soil interaction simulations [13,14].

The underlying principle of partsival and other DEM tools is the discretization of granular matter, hence the name of the method. The actual soil beneath the rover wheels on Phobos will consist of millions of small, irregularly shaped grains with greatly differing mechanical properties. The actual environment is far too complex to be simulated 1:1, hence requiring massive simplification. The microscopic grains are therefore implemented within partsival on a macroscopic level. An accumulation of many grains is discretized as spheres that replicate the macroscopic behavior of the granular material.

The interactions of these discretized spheres are then modeled by time integration of the Newtonian equations of momentum and motion. Despite the simplifications made, this is very computationally expensive. In order to not distort the simulation results, the discretized spheres must not represent a too large number of particles. Lichtenheldt developed in [15,16] a practical empiric equation to specify the maximum size of such a sphere that represents a compromise between minimal result distortion and computation time. The so-called tool resolution Γ can be calculated based on the dimensional properties of the wheel as follows:

$$\Gamma = \frac{L_{\min}}{2r_{\max}} \tag{1}$$

with $L_{\min}$, the characteristic tool dimension (in this case the grouser height) and the particle radius $r_{\max}$. Following Lichtenheldt, a conservative choice for the tool resolution when simulating wheels with grousers is $\Gamma = 5$.

The resulting particle bed still consists of more than 250 000 particles. Since the simulation is a full 3D simulation, each particle can be described by 6 equations, resulting in a total of over 1 500 000 equations that have to be solved for each time step. Since partsival is capable of highly parallelized computation on GPUs, the software is able to demonstrate its strengths and advantages.

1.2 Phobos Environment

Obviously, to simulate the behavior of the Phobos regolith, precise information on the regolith's mechanical properties is required. Amongst other parameters, partsival requires the regolith's grain size, Young's modulus, cohesive forces, friction angles, Poisson's ratio, the regolith's density and the gravitational acceleration of Phobos. Unfortunately, despite many missions aiming for Phobos, so far, no spacecraft was able to directly examine its surface. Therefore, there is no in-situ knowledge of the Phobos regolith.

Although the surface properties of Phobos are vastly unknown, thanks to remote observations they can at least be roughly quantified. The probably most precise information gained by remote sensing is the surface gravity of Phobos. However, the acceleration effective on Phobos' surface is not only determined by gravity. Due to the small distance to Mars and the small diameter of Phobos, tidal forces and centrifugal forces will affect the rover as well. Therefore, it is reasonable to use the term effective gravity, meaning a combination of those forces rather than taking only gravity into account. Effective gravity on Phobos is very low and fluctuates roughly between $3 \times 10^{-3}\,\mathrm{m/s^2}$ and $6.8 \times 10^{-3}\,\mathrm{m/s^2}$ [17]. However, due to the probable landing site choice, gravitational acceleration of over $5 \times 10^{-3}\,\mathrm{m/s^2}$ has to be expected [18].

As for the mechanical properties, only rough assumptions can be made. The thickness of the regolith layer on Phobos can be assumed by observing its craters and is believed to be several meters thick [17]. By assuming similar space weathering mechanisms such as micrometeorite bombardments [19] or thermal breakdown [20] as on other airless bodies, a good estimate of particle size and density can be made. The regolith layer on Phobos is probably composed of grains with a diameter ranging from 30 µm up to a few centimeters [5]. The bulk density of the upper regolith layer can be assumed in a range between $1.6\,\mathrm{g/cm^3}$ and $2.0\,\mathrm{g/cm^3}$ [17]. The grain density is believed to be around $2.6\,\mathrm{g/cm^3}$.

A good assumption for the angle of friction of the Phobos regolith can be made by observing the angle of repose of craters and dunes on Phobos. A good guess would be a friction angle of around 20 °. However, this guess follows assumptions regarding grain size and cohesion of the regolith and is therefore highly speculative.

The space weathering effects mentioned above, unfortunately, complicate a detailed determination of the surface material on Phobos. Thermal and spectral observations of Phobos are capable to narrow down potential surface compositions of Phobos. But since space weathering changes both, thermal and spectral properties of regolith, it is not possible to provide precise information [19]. There are three major theories regarding the surface composition of Phobos. The first hypothesis, supported by spectral analysis, suggests that the surface of Phobos consists of basaltic components with admixed phyllosilicates [21] or tectosilicates [22]. Since this composition is similar to the

Martian crust, it supports the theory of in-situ formation of the Martian moons after an impact event on Mars.

The second theory suggests, that Phobos consists of olivine and low-calcium pyroxene and is based on infrared spectral investigations. This assumption would support the hypothesis of the joint in-situ formation of the Martian moons with Mars itself. The last theory, which is currently considered most likely, suggests a composition of the Phobos regolith of carbonaceous chondrite, a carbon-rich silicate mixture frequently found in asteroids [23–26]. Thus, this theory supports the origin hypothesis of the moons of Mars as captured asteroids.

Since the surface composition of Phobos is not known, the mechanical properties of the soil are vastly unknown as well. However, based on the possible composition of Phobos, different scenarios for its surface can be created. To evaluate wheel traction on Phobos, we defined a worst-case scenario, based on powdery regolith. Since the cohesion of soil greatly affects its traversability, we investigate cohesive and non-cohesive soils. The mechanical properties used for the DEM simulation are presented in Table 1.1.

Table 1: DEM simulation parameters for powdery regolith

Parameter	Symbol	Value	Unit
effective gravity	$\overrightarrow{g_{\mathrm{eff}}}$	-6×10^{-3}	[m/s²]
particle diameter	d_{Grain}	30 to 70	[µm]
friction angle	Φ_{i}	20	[°]
grain density	ρ_{R}	2 600	[kg/m³]
Young's modulus	E	70	[GPa]
Poisson's ratio	ν_{R}	0.15	[-]
cohesion	c	0 to 1 000	[Pa]
tool-grain friction	Φ_{w}	18	[°]

2 OPTIMIZATION

After adjusting partsival to the environmental conditions of Phobos, we can perform the wheel optimization. Apart from the obvious goal of the wheel optimization, namely the improvement of traction, the influence of various geometry parameters is also to be determined. Therefore, geometry parameters and driving scenarios have to be defined.

As for driving scenarios, the definition is quite easy and tightly bound to the mission constraints and the experiences of previous rover missions like NASA's MER missions. The primary driving scenario is driving on level soil. Apart from that, the rover has to be capable of ascending slopes. Since the surface of Phobos is relatively smooth, the corresponding driving scenario utilizes a slope angle of 10 °. Even though slopes of up to 25 ° are to be expected on Phobos, the smaller gradient should rather correspond to the usual driving scenarios of the mission [17].

The third driving scenario covers the reversing capability of the rover. This is not only required in the event, that the rover has to leave hazardous zones backward as encountered by the Opportunity rover on Mars [27], but also for steering. The rover is meant to use point turns for steering instead of swing turns. Therefore, reversing will be a standard maneuver for the rover. The final scenario covers the more experimental question of multi-pass driving. This scenario is aimed at finding out if the front or rear wheels of the rover might need different wheel geometries to maximize traction, a question that has been raised before by others such as Lichtenheldt in [15].

Regarding geometry parameters, a whole lot of parameters could be taken into consideration. To avoid unnecessarily inflating the optimization campaign, only four geometry parameters are selected. The selection process of said parameters is based on the state of research on various geometry parameters to avoid unnecessary evaluations. Rover wheel and grouser parameters and their effect on traction is a well-studied field of research. Geometry parameters like the number or distribution of grousers on a wheel rim [7,9,10,13,28–31], the grouser height [7,10,11,13,28–31], width [13,31] and curvature [10,13,30] as well as wheel parameters like the curvature of the wheel rim (concave, flat or convex) [13], the wheel width [11,13] or the wheel diameter [7,13,28,29] are well researched and understood.

However, most research performed on the tractive influence of different rover wheel geometries is focused on wheeled locomotion in higher-gravity environments like Earth, Martian, or Lunar gravity. Research regarding wheeled locomotion in milli-g environments is still at the very beginning. Findings by Nakashima, Kobayashi [32], Lopez-Arreguin, Gundlach and Stoll [33] suggest, that wheel sinkage and motion resistance are connected to the gravitational acceleration. Adapting the wheel design to the gravitational environment of the deployment site is therefore necessary.

Since wheeled locomotion in milli-g environment can still be considered terra incognita, most research regarding rover wheel geometry cannot be applied to the MMX wheel design. Most geometry parameters like the number or height of grousers influence wheel slip and sinkage asymptotically or polynomial [12,13]. The optimal parameter value is therefore a non-extreme value and has to be determined depending on

environmental parameters like soil properties and gravity.

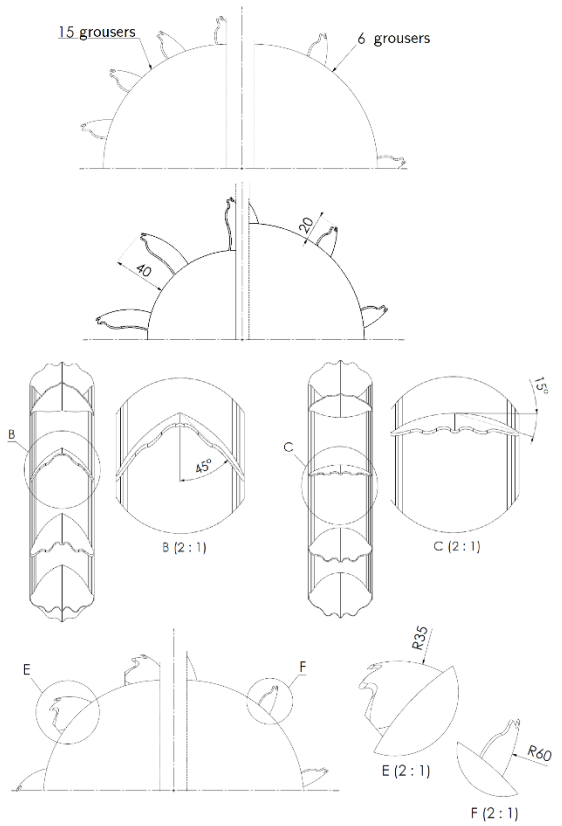

Figure 1: The examined geometry parameters

Only wheel diameter and wheel width can be optimized by choosing extreme parameter values. Traction will always increase with larger wheel width and diameter [13]. Wider rims distribute the rover weight on a larger surface and can therefore help to prevent soil failures underneath the wheel. The same applies to the wheel diameter when noticeable wheel sinkage occurs [13]. This relationship is also described by Equation 2, which allows an empirical determination of the rolling resistance R_R of rover wheels [34]:

$$R_R = K_U \sqrt{\frac{W_R^3}{b_R \cdot D_R^2}} \qquad (2)$$

with the wheel diameter denoted by D_R the wheel width b_R, the wheel mass W_R and the empiric soil parameter K_U. Since wheel width and diameter are restricted by space and weight requirements, traction can be optimized by choosing the maximal wheel width and diameter. An explicit optimization is therefore not necessary.

As a consequence, the geometry parameters number of grousers, grouser height and grouser curvature are adapted for use on Phobos. Additionally, a fourth geometry parameter, the grouser radius will be examined as well. To improve the comprehensibility of the parameters, Figure 1 shows all four geometry parameters with two different parameter values each. The first wheel illustrates grouser number changes. The left section shows a wheel with 15 grousers, while the right section shows a wheel with 6 grousers respectively. The second wheel shows the effect of alterations to the grouser height. Note, that since the maximum wheel diameter is capped, the grousers are enlarged at the expense of the wheel diameter. The next illustration shows the grouser curvature. With increasing grouser curvature angle, the grousers form a V- or chevron shape. Lastly, the bottom illustration shows how changes to the grouser radius influence the grouser shape. An increasing grouser radius leads to grousers in the shape of a quarter circle with a partially closed geometry.

2.1 Simulation Setup

To reduce the size of the particle bed and therefore the number of discrete element particles within the simulation runs, only single wheel simulations will be performed. A further reduction of particles being actively simulated is achieved by exploiting wheel symmetry and dynamic boundaries. Since the rover wheel can be simplified considered symmetrical, the computational domain and therefore the number of particles can shrink by 50 %. The symmetry domain halves the rover wheel in the middle of the wheel width. The particle velocity V_s left (−) and right (+) hand of the symmetry plane therefore evaluates to [13,15]:

$$|\Delta V_s| \to 0 \;\forall\; \Delta V_s = V_s^+ - V_s^-; \wedge\; |V_s^+| \cong |V_s^-|; \qquad (3)$$

Friction forces between particles right and left hand of the symmetry plane can therefore be neglected, resulting in a frictional interface evaluating to [13,15]:

$$|F_R^{\pm}| = 0 \quad \to \quad \mu_r^{\pm} = 0 \qquad (4)$$

The dynamic boundaries are computational domain boundaries whose movements are linked to the tool or wheel movement. Thus, particles that are too far away from the wheel to be affected by its movement are not included in the computation [15]. The dimensions of the soil bed also depend on the influence area of the wheel and furthermore on the travel distance of the wheel. Since two wheel revolutions are considered suitable to compensate for fluctuations in the simulation process [15], the soil bed needs to be at least 0.8 m long. The width and height of the soil bed are 0.085 m and 0.13 m respectively, resulting in an overall particle count of 250 000 particles [12].

To precisely measure the locomotion capabilities of a rover wheel design, average values will be evaluated. Settling behaviors like static sinking can therefore be neglected [12]. However, this raises the need for longer simulation runs. In order to achieve a steady state, the rover wheel has to perform at least one full revolution. Further revolutions can be considered advantageous [15]. Two wheel revolutions will be performed with each simulation run to minimize the influence of settling effects. The MMX rover's wheels will revolve on Phobos with a velocity of approx. 0.25 rad/s, resulting in a theoretical velocity of 2.675 cm/s [12]. To achieve two wheel revolutions, the wheel will have to revolve for at least 50 s, not considering settling and acceleration time. The overall simulation time is therefore chosen to be 65 s [12]. With an average time step size of 1×10^{-4} s, a single simulation requires the computation of approximately 650 000 time steps.

The performance parameters used to evaluate wheel designs are slip and sinkage. The drawbar pull, which is utilized in many other publications to evaluate the performance of a wheel, is not used. This is because the MMX rover is a four-wheel-drive vehicle. The pulling power of the rover is therefore not of particular interest. Furthermore, the expected wheel slip is not known. Realistic drawbar-pull evaluation is hence not possible. In summary, the simulations are carried out as single wheel experiments with fixed angular velocity and free slip.

2.2 Strategy

The optimization strategy applied in this work focusses more on the observation of the effects of parameter changes rather than on an extensive optimization. The effects of single parameter changes can serve as a benchmark for future wheel developments in similar environments. Therefore, the four geometry parameters are varied individually. The mutual influence of different parameters can hence not be observed.

The experiment design reflects this choice. Instead of extensive optimization strategies such as factorial or algorithm-driven experiment designs, a one-factor-at-a-time (OFAT) experimental approach is applied. The OFAT optimization is based upon an intermediate design model, driven by the engineering experience at the Institute for System Dynamics and Control at the German Aerospace Center.

Since the geometry parameters are not independent variables, only a local optimal wheel design can be identified. However, the chosen approach enables the observation of parameter influence and importance and therefore enables the development of design guidelines for rover wheels in milli-g environments.

Due to the choice of experimental design, the simulation results might depend on the order in which the parameters are varied. This is why a more thorough follow-up wheel optimization with generic wheels is already in progress at DLR.

3 OPTIMIZATION RESULTS

For every wheel simulation, wheel slip and wheel sinkage for each time step can be stored for later evaluation. Since the wheel simulations with partsival heavily rely on GPU parallelization, result deviation when repeating simulation runs is a well-known issue [35]. However, partsival being a highly adaptable simulation framework can be modified to fit the specific numerical needs of simulations in milli-g environments. With modifications to its numerical precision and its integration scheme parameters, partsival can deliver simulation results with minimal, non-macroscopic deviation [12].

Based on the results of single simulation runs, wheel slip, wheel travel capabilities and average wheel sinkage can be determined. Based on repeated simulation runs and the assumption of normally distributed simulation errors [12], confidence intervals for each simulation run can be calculated, indicating the probability of erroneous simulation results. The simulation result's average values are shown as circles. The upper and lower confidence intervals for 90 % confidence are shown as asterisks. Furthermore, since the wheel geometry parameters are changed incrementally, trendlines can be visualized using a least-squares approximation algorithm.

The first wheel parameter being changed is the grouser radius. The radius is changed in increments of 5 °, ranging from 35 ° to 80 °, covering a broad range from almost straight grousers to grousers with a quarter circle shape. Figure 2 shows the results to said incremental parameter changes in four different scenarios. The upper graphs show the parameter's influence on wheel travel and therefore indicating the magnitude of wheel slip, while the lower graphs show the influence on wheel sinkage. The four different driving scenarios are depicted in different colors and line styles.

The first parameter, the grouser radius, has very little influence on wheel sinkage. Regarding wheel travel, an increasing grouser radius does improve locomotion. When traversing soil in reverse, the grouser radius has minimal influence on traction. In summary, locomotion improves with an increasing grouser radius. Since the grousers become asymptotically straight with a

larger radius, a non-bent grouser is optimal regarding wheel traction.

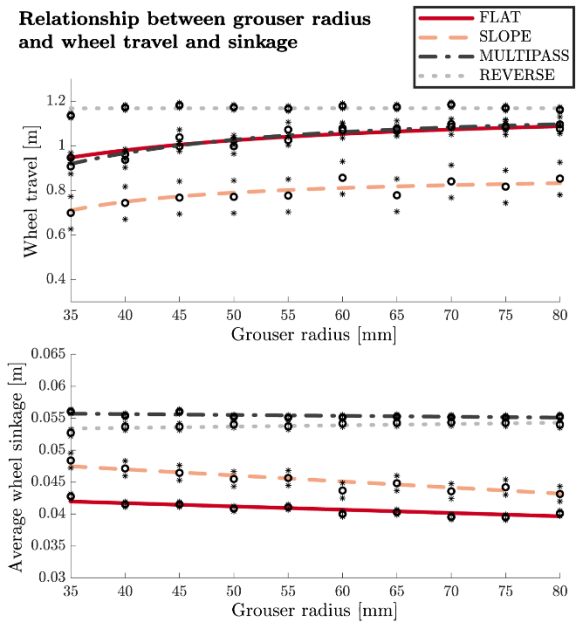

Figure 2: Grouser radius and wheel traction

Since non-bent grousers optimize traction, the second parameter, the grouser curvature is examined with straight grousers. The curvature is also changed in 5 ° increments ranging from 0 °, so non-curved grousers to 45 ° curved grousers. Examination of angles greater than 45 ° is not necessary, since the wheel is driven backward in the reverse driving scenario. The grouser chevron therefore engages with the soil at a −45 ° angle. The results of the grouser curvature variation are depicted in Figure 3.

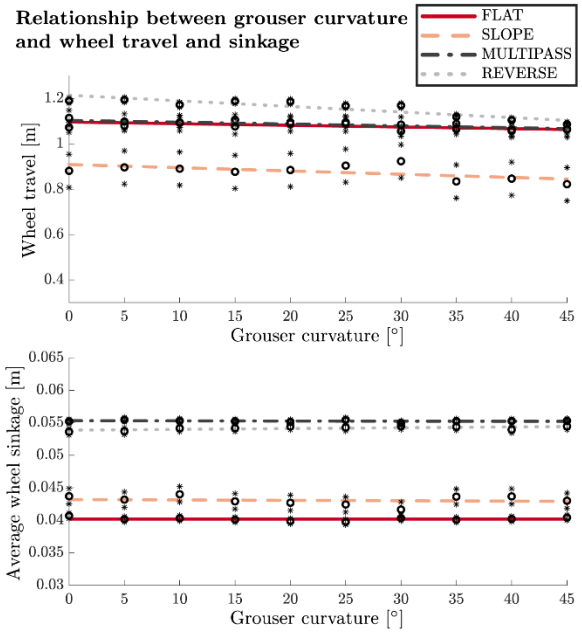

Figure 3: Grouser curvature and wheel traction

Similarly to the grouser radius, the grouser curvature has little effect on wheel traction. Only when driving reverse, curvature impedes wheel travel. So, a positive grouser curvature angle neither improves nor worsens locomotion capabilities when driving forward but worsens wheel traction in reverse. Therefore, non-curved grousers improve wheel locomotion and the next geometry parameter, the grouser height is examined with non-curved grousers.

In contrary to both previous geometry variations, the grouser height has a tremendous effect on a wheel's locomotion capabilities. However, the influence of a changing grouser height is ambiguous. With increasing height, wheel slip can be reduced, leading to higher wheel travel with given wheel revolutions. Higher grousers can penetrate deeper into the soil, increasing the contact surface between wheel and soil which can ultimately help to prevent soil failure [13]. This increase in traction is limited though. Since the maximum wheel diameter is capped, the grouser height changes at the expense of the rim diameter. When the wheel rolls over its rim, the lower wheel circumference leads to less travel distance. Figure 4 shows these results.

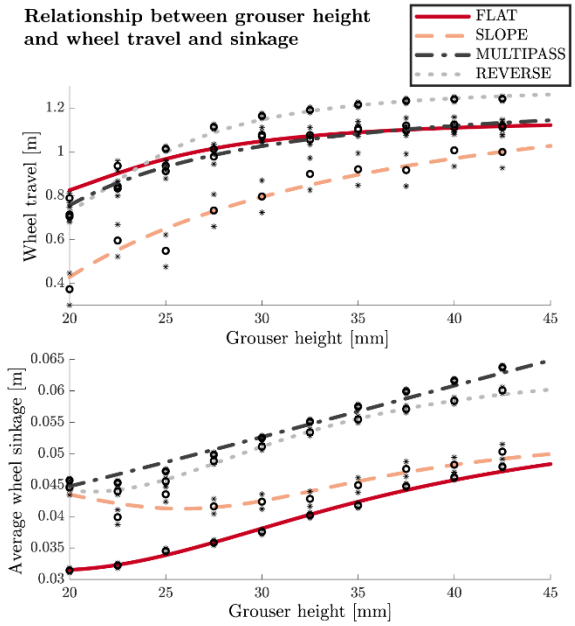

Figure 4: Grouser height and wheel traction

On the other hand, deeper penetration of the grousers obviously also increases wheel sinkage. Therefore there can't be an optimal grouser height. The grouser height must rather be chosen as a compromise between traction and sinkage. In this case, we chose a grouser height of 35 mm. The last geometry parameter variation, the number of grousers, therefore commences with said grouser height.

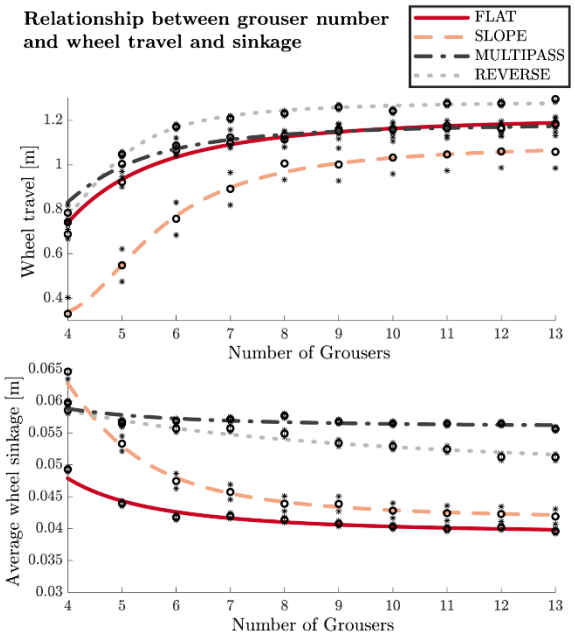

Figure 5: Grouser number and wheel traction

The grouser number, as depicted in Figure 5, has the largest effect on wheel locomotion capabilities. The grouser number is varied in this study from four grousers per wheel to thirteen grousers per wheel. It shows to have a similar effect on wheel travel and wheel sinkage. With an increasing grouser number, wheel travel increases, while slip and wheel sinkage gradually decrease. However, this parameter shows an asymptotic course. Depending on the scenario, more than eight to ten grousers do not significantly improve locomotion capabilities anymore. For reasons of weight economy, the rover wheel should therefore be equipped with eight to ten grousers. In the given case of the MMX rover, we opt for ten grousers per wheel.

4 CONCLUSION AND OUTLOOK

The primary result of the optimization campaign is an improved rover wheel design that reduces slip and sinkage for a rover deployed on Phobos. Even if the rover wheel is not fully optimized yet, the improved rover wheel easily outperforms the intermediate design model. Further optimization involving generic rover wheels and considering the mutual influence of geometry parameters will be performed at DLR. The transition from intermediate wheel design to partially optimized wheel and grouser geometry is depicted in Figure 6.

The optimized rover wheel is characterized above all by straight, very high grousers. The rounded, shell-shaped structure of the intermediate design is eliminated as well. Those changes alone result in about 50 % less slip when traversing loose soils.

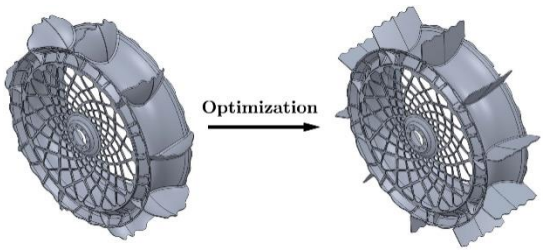

Figure 6: From intermediate design to optimized wheel

While the intermediate wheel design showed about 20 % of slip, the optimized wheel reduced slip to only 10 %. When traversing cohesive soils, the rover's locomotion capability improves even further.

Additionally, the results presented in this paper can also serve as a benchmark and design guideline on how to adapt rover wheels to milli-g environments. The graphs show the influence of incremental grouser geometry variations and should enable engineers in similar projects to develop a solid first design. Furthermore, this work shows, that rover wheel design for milli-g environments does not differ significantly from designing rover wheels for higher gravity environments. For example, the findings presented by Ono in [13] mostly match with the findings of this paper. The optimal grouser number mostly depends on wheel diameter, driving scenario and environment and therefore needs adaptation to its environment. Regarding grouser curvature and radius, milli-g environments do not differ at all from other environments. Additionally, the grouser height has to be adapted for lower gravity. Since the normal forces acting on the ground beneath the rover wheels are lower due to the reduced gravity, friction between wheel and ground decreases as well. Therefore, additional friction has to be generated by higher grousers penetrating the soil. [12]

References

[1] P. Rosenblatt, "The origin of the Martian moons revisited," *The Astronomy and Astrophysics Review*, vol. 19, no. 1, 2011.

[2] W. K. Hartmann, "Additional evidence about an early intense flux of C asteroids and the origin of Phobos," *Icarus*, vol. 87, no. 1, pp. 236–240, 1990.

[3] J. A. Burns, "Dynamical characteristics of Phobos and Deimos," *Reviews of Geophysics*, vol. 10, no. 2, p. 463, 1972.

[4] S. Tardivel and C. Lange, "The MMX Rover: An Innovative Design Enabling Phobos in-situ Exploration," in *13th IAA Low-Cost Planetary Missions Conference*, 2019.

[5] A. T. Basilevsky, C. A. Lorenz, T. V. Shingareva et al., "The surface geology and geomorphology of Phobos," *Planetary and Space Science*, vol. 102, pp. 95–118, 2014.

[6] H. Miyamoto, T. Niihara, K. Wada et al., "Phobos Environment Model and Regolith Simulant for

MMX Mission," in *49th Lunar and Planetary Science Conference*, USRA Houston, 2018.

[7] K. Skonieczny, S. J. Moreland, and D. S. Wettergreen, "A Grouser Spacing Equation for Determining Appropriate Geometry of Planetary Rover Wheels," in *IEEE/RSJ International Conference on Intelligent Robots and Systems*, 2012.

[8] R. E. Arvidson, J. F. Bell, P. Bellutta et al., "Spirit Mars Rover Mission: Overview and selected results from the northern Home Plate Winter Haven to the side of Scamander crater," *Journal of Geophysical Research: Planets*, vol. 115, E12, p. 821, 2010.

[9] M. Sutoh, K. Nagaoka, K. Nagatani et al., "Design of wheels with grousers for planetary rovers traveling over loose soil," *Journal of Terramechanics*, vol. 50, no. 5, pp. 345–353, 2013.

[10] H. Inotsume, S. Moreland, K. Skonieczny et al., "Parametric study and design guidelines for rigid wheels for planetary rovers," *Journal of Terramechanics*, vol. 85, pp. 39–57, 2019.

[11] O. A. Ani, H. Xu, Y.-p. Shen et al., "Modeling and multiobjective optimization of traction performance for autonomous wheeled mobile robot in rough terrain," *Journal of Zhejiang University SCIENCE C*, vol. 14, no. 1, pp. 11–29, 2013.

[12] F. Buchele, *Optimierung der Traktion eines planetaren Rovers mit der Diskreten Elemente Methode*, Master's Thesis, University of Applied Sciences Kempten, 2020.

[13] S. Ono, *Evaluation of Planetary Rover Wheel Performance on Sloped Loose Soil Based on Discrete Element Method*, Master's Thesis, Tohoku University, 2019.

[14] R. Lichtenheldt, S. Kerler, A. Angerer et al., "partsival - Collision-based Particle and many-body Simulations on GPUs for Planetary Exploration Systems," in *The 5th Joint International Conference on Multibody System Dynamics*, 2018.

[15] R. Lichtenheldt, *Lokomotorische Interaktion planetarer Explorationssysteme mit weichen Sandböden*, Doctoral thesis, Technische Universität Ilmenau, 2016.

[16] R. Lichtenheldt and B. Schaefer, "Locomotion on Soft Granular Soils: A Discrete Element based Approach for Simulations in Planetary Exploration," in *12th Symposium on Advanced Space Technologies in Robotics and Automation*, 2013.

[17] R. O. Kuzmin and E. V. Zabalueva, "The Temperature Regime of the Surface Layer of the Phobos Regolith in the Region of the Potential Fobos–Grunt Space Station Landing Site," *Solar System Research*, vol. 37, no. 6, pp. 480–488, 2003.

[18] J. Bertrand, S. Tardivel, F. Ijpelaan et al., "Roving on Phobos: Challenges of the MMX Rover for Space Robotics," in *15th Symposium on Advanced Space Technologies in Robotics and Automation*, 2019.

[19] C. M. Pieters and S. K. Noble, "Space weathering on airless bodies," *Journal of Geophysical Research: Planets*, vol. 121, no. 10, pp. 1865–1884, 2016.

[20] M. Delbo, G. Libourel, J. Wilkerson et al., "Thermal fatigue as the origin of regolith on small asteroids," *Nature*, vol. 508, no. 7495, pp. 233–236, 2014.

[21] T. D. Glotch, C. S. Edwards, M. Yesiltas et al., "MGS-TES Spectra Suggest a Basaltic Component in the Regolith of Phobos," *Journal of Geophysical Research: Planets*, vol. 123, no. 10, pp. 2467–2484, 2018.

[22] M. Giuranna, T. L. Roush, T. Duxbury et al., "Compositional interpretation of PFS/MEx and TES/MGS thermal infrared spectra of Phobos," *Planetary and Space Science*, vol. 59, no. 13, pp. 1308–1325, 2011.

[23] A. A. Fraeman, R. E. Arvidson, S. L. Murchie et al., "Analysis of disk-resolved OMEGA and CRISM spectral observations of Phobos and Deimos," *Journal of Geophysical Research: Planets*, vol. 117, E11, 2012.

[24] A. A. Fraeman, S. L. Murchie, R. E. Arvidson et al., "Spectral absorptions on Phobos and Deimos in the visible/near infrared wavelengths and their compositional constraints," *Icarus*, vol. 229, pp. 196–205, 2014.

[25] K. D. Pang, J. B. Pollack, J. Veverka et al., "The composition of Phobos - Evidence for carbonaceous chondrite surface from spectral analysis," *Science*, 1978.

[26] A. S. Rivkin and R. H. Brown, "Near-Infrared Spectrophotometry of Phobos and Deimos," *Icarus*, vol. 156, no. 1, pp. 64–75, 2002.

[27] R. E. Arvidson, J. W. Ashley, J. F. Bell et al., "Opportunity Mars Rover mission: Overview and selected results from Purgatory ripple to traverses to Endeavour crater," *Journal of Geophysical Research: Planets*, vol. 116, E10, p. 3845, 2011.

[28] S. Jayalekshmi and P. Gireesh Kumar, "Studies on the sinkages of rigid plain wheels and lugged wheels on TRI-1 lunar soil simulant," *Journal of Terramechanics*, vol. 82, pp. 35–42, 2019.

[29] M. Sutoh, J. Yusa, T. Ito et al., "Traveling performance evaluation of planetary rovers on loose soil," *Journal of Field Robotics*, vol. 29, no. 4, pp. 648–662, 2012.

[30] Y. Du, J. Gao, L. Jiang et al., "Numerical analysis of lug effects on tractive performance of off-road wheel by DEM," *Journal of the Brazilian Society of Mechanical Sciences and Engineering*, vol. 39, no. 6, pp. 1977–1987, 2017.

[31] H. Nakashima, H. Fujii, A. Oida et al., "Parametric analysis of lugged wheel performance for a lunar microrover by means of DEM," *Journal of Terramechanics*, vol. 44, no. 2, pp. 153–162, 2007.

[32] H. Nakashima and T. Kobayashi, "Effects of gravity on rigid rover wheel sinkage and motion resistance assessed using two-dimensional discrete element method," *Journal of Terramechanics*, vol. 53, pp. 37–45, 2014.

[33] A.J.R. Lopez-Arreguin, B. Gundlach, and E. Stoll, "Do lunar rover wheels sink equally on Earth and Moon?," *Results in Physics*, vol. 15, 2019.

[34] T. Tanaka and A. Oida, *Sharyō kikai to dokei no rikigaku*: *Teramekanikkusu*, Gakubunsha, 1993.

[35] N. Kapre and A. DeHon, "Optimistic Parallelization of Floating-Point Accumulation," in *IEEE Symposium on Computer Arithmetic*, 2007.